



This is a repository copy of *Study of the luminescence decay of a semipolar green light-emitting diode for visible light communications by time-resolved electroluminescence*.

White Rose Research Online URL for this paper:

<https://eprints.whiterose.ac.uk/188909/>

Version: Published Version

Article:

Holly Hagggar, J.I., Ghataora, S.S., Trinito, V. et al. (2 more authors) (2022) Study of the luminescence decay of a semipolar green light-emitting diode for visible light communications by time-resolved electroluminescence. *ACS Photonics*, 9 (7). pp. 2378-2384. ISSN 2330-4022

<https://doi.org/10.1021/acsp Photonics.2c00414>

Reuse

This article is distributed under the terms of the Creative Commons Attribution (CC BY) licence. This licence allows you to distribute, remix, tweak, and build upon the work, even commercially, as long as you credit the authors for the original work. More information and the full terms of the licence here:

<https://creativecommons.org/licenses/>

Takedown

If you consider content in White Rose Research Online to be in breach of UK law, please notify us by emailing eprints@whiterose.ac.uk including the URL of the record and the reason for the withdrawal request.



eprints@whiterose.ac.uk
<https://eprints.whiterose.ac.uk/>

Study of the Luminescence Decay of a Semipolar Green Light-Emitting Diode for Visible Light Communications by Time-Resolved Electroluminescence

Jack Ivan Holly Hagggar, Suneal S. Ghataora, Valerio Trinito, Jie Bai, and Tao Wang*



Cite This: <https://doi.org/10.1021/acsp Photonics.2c00414>



Read Online

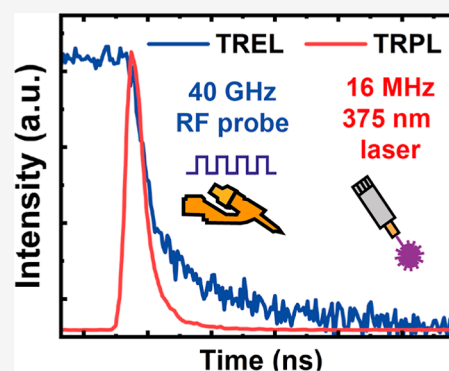
ACCESS |

Metrics & More

Article Recommendations

ABSTRACT: Time-resolved photoluminescence (TRPL) is often used to study the excitonic dynamics of semiconductor optoelectronics such as the carrier recombination lifetime of III-nitride light-emitting diodes (LEDs). However, for any real-world application that requires LEDs under electrical injection, TRPL suffers an intrinsic limitation due to the absence of taking carrier transport effects into account. This becomes a severe issue for III-nitride LEDs used for visible light communication (VLC) since the modulation bandwidth for VLC is determined by the overall carrier lifetime of an LED, not just its carrier recombination lifetime. Time-resolved electroluminescence (TREL), which can characterize the luminescence decay of an LED under electrical injection to simulate real-world conditions when used in practical applications, is required. Both TRPL and TREL have been carried out on a semipolar LED and a standard c-plane LED (i.e., polar LED) both in the green spectral region for a comparison study. The (11-22) green semipolar LED exhibits much faster differential carrier lifetimes than the c-plane LED. In addition to a fast exponential component and a slow exponential component of 0.40 and 1.2 ns, respectively, which are similar to those obtained by TRPL, a third lifetime of 8.3 ns due to transport-related effects has been obtained from TREL, which has been confirmed by capacitance measurements. It has been found that the overall carrier lifetime of a c-plane LED is mainly limited by RC effects due to a junction capacitance, while it is not the case for a semipolar LED due to intrinsically reduced polarization, demonstrating the major advantages of using a semipolar LED for VLC.

KEYWORDS: InGaN, GaN, LED, TREL, TRPL, VLC



INTRODUCTION

There is an increasing demand for developing a visible light communication (VLC) technology that is based on a visible emitter [either a light-emitting diode (LED) or a laser diode] as a transmitter, an emerging wireless communication technology offering a complementary approach to radio frequency (RF)-based Wi-Fi and 5G. As a result of using visible light, whose wavelength is much shorter than those of RF, the frequency bandwidth is more than 3 orders of magnitude larger than those for RF. It has been predicted that VLC provides a long-term solution to the looming RF “spectrum crunch” due to a substantial increase in data demand.¹

A data transmission rate is largely determined by the bandwidth of a transmitter and the signal-to-noise ratio of a receiver. A high data transmission rate requires a visible emitter with both high output power and a short carrier lifetime. Time-resolved photoluminescence (TRPL) is a powerful tool for characterizing a carrier recombination lifetime but is fundamentally confined to the active region of an emitter and does not contain information about carrier transport through the emitter structure, active region carrier density, or

performance when considering real-world LED applications under biasing conditions (i.e., electrical injection).^{2–4} Therefore, it is crucial to explore a method that allows us to study the carrier dynamics of an emitter under biasing conditions for VLC applications.

In general, the modulation bandwidth of an LED (labeled as f) is inversely proportional to the overall carrier lifetime of an LED (labeled as τ), that is, $f \propto 1/\tau$, which can be described by eq 1 given below

$$f \propto \frac{1}{\tau} = \frac{1}{\tau_r} + \frac{1}{\tau_{nr}} + \frac{1}{\tau_{RC}} \quad (1)$$

where τ_r is the lifetime due to radiative recombination and τ_{nr} the lifetime due to nonradiative recombination. It is worth

Received: March 14, 2022

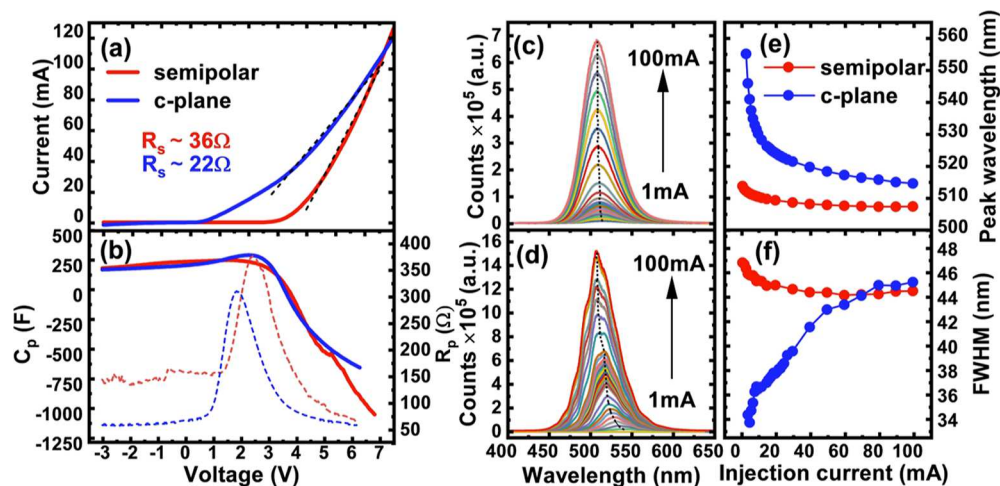


Figure 1. Electrical and optical characteristics of the semipolar LED and the c-plane LED: I – V curves and series resistance (a); capacitance (solid) and resistance (dashed) measured using an LCR meter in a parallel circuit mode at 1 MHz (b); EL spectra of the semipolar LED as a function of injection current (c); EL spectra of the c-plane LED as a function of injection currents (d); peak wavelength shift of both LEDs as a function of injection current (e); and FWHM of the EL spectra of the both LEDs as a function of injection current (f).

highlighting that the third component labeled as τ_{RC} is the lifetime due to the junction capacitance of an emitter, that is, the so-called RC effects (i.e., resistance labeled as R and junction capacitance labeled as C). The junction capacitance of an emitter sensitively depends on its dimension. The dimension of a standard III-nitride LED is $>300 \mu\text{m} \times 300 \mu\text{m}$. Generally speaking, an emitter with an area of $<100 \mu\text{m}^2$ is not limited by τ_{RC} in terms of overall carrier lifetime and modulation bandwidth for VLC applications.^{5–8} However, broader-area LEDs are desirable in terms of easier fabrication, higher optical power, and cheaper integration solutions, where it is essential to consider τ_{RC} if they are used for VLC applications.

τ_r and τ_{nr} are normally studied and can be separated by means of using temperature-dependent TRPL measurements with the assumption that τ_{nr} can be safely negligible at a low temperature.⁴ This method, while being sufficient for the optical investigation of an emitter under optical pumping conditions, does not tell the whole story for an emitter under biasing conditions since TRPL completely neglects carrier transport effects. Moreover, since TRPL is performed under optical pumping, it is challenging to quantify the carrier density in the active region of an emitter. Therefore, τ_r only provides an approximate characterization since $\tau_r = 1/BN$, where B is the recombination coefficient and N is the carrier density.⁹ There is an alternative to TRPL, namely, time-resolved photocurrent, which has been applied to the investigation of transport effects of GaInP solar cells.¹⁰ For InGaN LEDs under electrical injection for VLC applications, electroluminescence (EL) measurements are essential.

In an ideal case, the luminescence decay of an LED should be characterized under electrical injection to simulate real-world conditions when used in practical applications. Therefore, time-resolved electroluminescence (TREL) measurements as a function of bias will allow us to accurately investigate the decay dynamics of an LED for practical applications, which is particularly important for VLC applications. TREL demonstrates two major benefits. The excitation signal (electrically injected square wave with an ultrafast falling edge) used for TREL is described as a small perturbation compared to the DC bias used to electrically drive

an LED, that is, dR/dN . The resulting lifetimes measured are therefore *differential lifetimes* instead of carrier recombination lifetimes measured from TRPL, with the latter being around 2–3 times smaller than the former.^{10,11} The carrier density in the active region can be then calculated by simply integrating the differential lifetime across the thickness of the active region, from which a physical model can be applied to the resulting response.

The differential carrier lifetime has been studied extensively using various methods for optoelectronics with most reports based on vector network analyzers, where both the impedance and the optical modulation response of an LED can be measured and both responses can be fit simultaneously to a physical model.^{11–15} The optical receivers are usually silicon-based photodetectors with either integrated transimpedance amplifiers or separate operational amplifiers that intrinsically suffer from low responsivity in the visible spectral range (e.g., 0.1 A/W at 450 nm). As III-nitride emitters used as transmitters for VLC applications are approaching the limit of these detectors,^{16–18} recent efforts have been focused on finding new alternatives for the receivers in VLC characterization systems. By means of using a combination of time-correlated single photon counting (TCSPC) electronics and hybrid photomultiplier tubes (PMTs), which are similar to what are used in TRPL, we can establish an electrically injected time-resolved system that exhibits high sensitivity with impulse responses of <50 ps compared with conventional photodetectors used in frequency domain systems.

There are also key issues associated with commercially available LEDs used for VLC. Commercially available white LEDs are typically fabricated by using polar orientated III-nitride blue LEDs grown on c-plane substrates coupled with yellow phosphors as conversion layers, where such an LED suffers greatly from strain-induced piezoelectric fields across the InGaN/GaN multiple quantum well (MQW) emitting region.^{19,20} The blue LEDs experience a reduced overlap between the electron–hole wavefunctions, leading to a long radiative recombination time and thus low quantum efficiency, that is, the so-called quantum confined Stark effect (QCSE). The color conversion process is also very slow, resulting in increased response lifetimes.²¹ Replacing the phosphor layers

by longer wavelength emitters such as yellow or red LEDs results in an even larger strain across the InGaN MQWs and therefore an enhanced QCSE, which further increases the carrier recombination lifetime. Growing III-nitride LEDs along a semipolar or nonpolar orientation, such as the LEDs grown on (11-22) semipolar substrates, has been proposed to naturally minimize or even eliminate the QCSE, effectively increasing the recombination rate.²² The (11-22) orientation also facilitates the enhancement of indium incorporation into InGaN, enabling longer-wavelength emitters along with a reduction in polarization.²³

Recently, we have demonstrated record breaking modulation bandwidths and multi-gigabyte per second data transmission rates for our large-area semipolar LEDs up to the amber spectral region.^{11,25} In this paper, we explore further into the nature of semipolar LEDs due to reduced polarization and their benefits for VLC. In this paper, both TREL and TRPL measurements have been performed on two different kinds of green LEDs, one grown on c-plane sapphire and the other grown on our high-quality semipolar (11-22) GaN overgrown on m-plane sapphire substrates.²⁴ Interestingly, we have found that even though RC measurements suggest that both the c-plane LED and the semi-polar LED should be limited by τ_{RC} , only the c-plane LED suggests that τ_{RC} is a limiting factor, while the TREL data from the semipolar LED are comparable to their TRPL results. Our results have shown that the semipolar LED demonstrates an increased recombination rate compared with the c-plane LED. More importantly, it has been found out that RC effects exhibit less contribution to the overall carrier lifetime for the semipolar LED than that for the c-plane LED, demonstrating the major advantage of using semipolar LEDs for VLC applications compared with c-plane LEDs.

RESULTS AND DISCUSSION

Figure 1a shows the current–voltage (I – V) characteristics of both the semipolar LED and the c-plane LED, indicating turn-on voltages (measured at 20 mA) of 4.3 and 2.5 V with corresponding series resistances of 36 and 22 Ω for the semipolar LED and the c-plane LEDs, respectively. Figure 1b exhibits the capacitance and resistance of these two LEDs measured using a precision LCR meter at 1 MHz in a parallel circuit mode, where the capacitance of an LED is given by its depletion capacitance below 0 V.²⁷ Therefore, the RC time constant of each LED can be obtained using the series resistance and the depletion capacitance under a negative bias. In this case, capacitance values of 194 and 173 pF have been measured at -2 V, corresponding to RC time constants of 7.0 and 3.8 ns for the semipolar LED and the c-plane LEDs, respectively. It is worth highlighting that these values are an approximate for the real RC lifetime and only serve as a lower limit due to the nonlinearity of the devices. Based purely on these measurements, however, if the carrier lifetime is in fact found to be dominated by the RC lifetime (as the typical size of a standard LED is $>300 \times 300 \mu\text{m}^2$) when electrically injected, we would expect the c-plane LED to exhibit a faster decay time when measured on the time-resolved system.

Figure 1c,d shows the EL spectra of the two LEDs measured as a function of the injection current for the semipolar LED and the c-plane LEDs, respectively. At 100 mA, both LEDs exhibit similar peak wavelengths of 507 and 514 nm for the semipolar LED and the c-plane LEDs, respectively. Due to the reduced QCSE, the emission wavelength shift of the semipolar

LED is only 7 nm, compared with 40 nm for the c-plane LED when measured between 1 and 100 mA, as shown in Figure 1e. Similarly, Figure 1f displays that the full width at half maximum (FWHM) of the semipolar LED experiences a 3 nm narrowing at the injection current of up to around 60 mA due to the naturally reduced polarization and then broadens slightly at higher injection currents mainly due to band filling effects. In contrast, the c-plane LED experiences an 11 nm broadening between 1 and 100 mA due to QCSE and band filling effects. This has been often observed in III-nitride c-plane LEDs.

Figure 2a shows the results of TRPL measurements performed on both samples at room temperature. A bi-

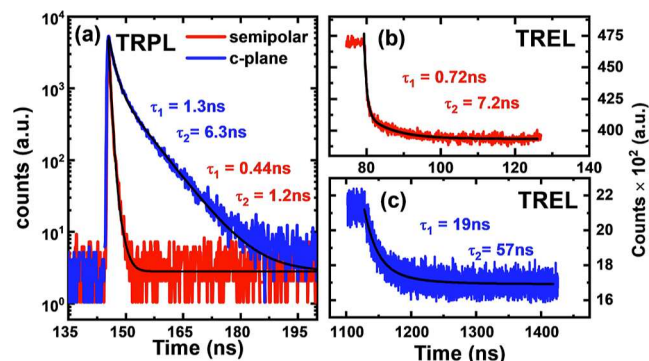


Figure 2. TRPL decay traces and fitting with a bi-exponential model showing extracted lifetimes for both the semipolar LED and the c-plane LED (a) and TREL decay traces for the semipolar LED (b) and c-plane (c) LED with the same bi-exponential model applied with associated extracted lifetimes.

exponential model is typically employed to fit the decay trace of InGaN, namely, a fast exponential component and a slow exponential component to fit the decay traces.^{2–4,28,29} This behavior is usually due to two radiative recombination channels contributing to the decay. The exciton binding energy of GaN is large (>26 meV), meaning that room-temperature excitons and carrier localization effects are the main factors contributing toward the bi-exponential nature of the decay.^{30–32} The extracted lifetimes from the TRPL data are 0.44 and 1.3 ns for τ_1 and 1.2 and 6.3 ns for τ_2 corresponding to the semipolar and c-plane LEDs, respectively. It is clear that the semipolar LED exhibits much faster lifetimes for both fast and slow components, which are attributed to a reduction in QCSE, allowing an enhanced recombination rate. However, for VLC applications that require fast LED switching speeds under electrical injection, TRPL results are not enough to confirm high performance as TRPL neglects carrier transport effects through the LED structure. We therefore extend this measurement further by electrically injecting the device and observing the EL decay dynamics over time. Figure 2b,c show the results of TREL decay traces of the two LEDs both measured at room temperature, which will be discussed later on.

Figure 3a shows the experimental setup for our TREL system. Figure 3b shows a typical example for an electrical input waveform generated by an arbitrary wave generator (AWG) as an excitation source and the resulting histogram waveform acquired over time from a PMT detector displaying the LED recombination dynamics. For the semipolar LED, a 500 mV (peak-to-peak) waveform with a repetition rate of 10 MHz (100 ns) is used as an excitation source, while an

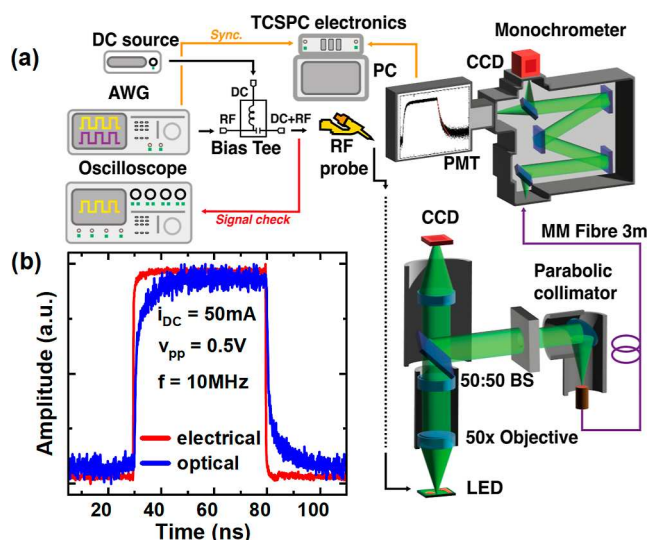


Figure 3. Schematic of our TREL system (a) and typical electrical input signal (red) from an AWG measured on an RF oscilloscope and the measured output (blue) from a PMT (b).

identical but less frequent 1 MHz (1000 ns) source is used for the c-plane LED. The lower frequency for the c-plane LED is necessary for the device to reach a steady state before measuring decay dynamics. In any time-resolved system, the instrument response function (IRF) needs to be taken into consideration. Since it is very difficult to directly measure the IRF of a system such as this, which takes both the electrical and optical sides into account simultaneously (this would require a probe-able, electrically injected emitter operating at >500 nm with picosecond response times), we outline the response times of each major component in the system in Table 1, which should serve as a good approximation of the IRF. The IRF is approximated to be ~ 67 ps, calculated using the sum of the squares of each component's response time.

Table 1. Response Time of Each Component of Our TREL System to Estimate the IRF

component	response time (ps)
AWG	22
Bias Tee	30
TCSPC electronics	6.5
RF probe	25
PMT	<50
RF cables	38

Figure 2b,c shows the TREL traces of the two LEDs and their corresponding fitting results for a typical waveform biased at 50 mA for both LEDs. Initially, a bi-exponential model similar to that we used for TRPL was employed to fit the decay curves of both LEDs, aiming to approximately compare the two types of measurements. In this case, the extracted lifetimes from the TREL data are 0.72 and 19 ns for τ_1 and 7.2 and 57 ns for τ_2 corresponding to the semipolar LED and the c-plane LEDs, respectively. This direct comparison shows that there are much larger differences between the two LEDs than for TRPL, with the semipolar LED experiencing similar but slightly higher lifetimes than on TRPL and the c-plane LED showing much higher lifetimes.

In addition to the bi-exponential behavior commonly observed in InGaN photoluminescence decay stemming from different radiative recombination channels such as excitonic contributions and carrier localization, a slower third term encompassing various carrier transport-related recombination mechanisms in the cladding and barrier layers, defects, and junction capacitance-related effects is added for TREL measurements.

Figure 4a,b shows the TREL traces of the semipolar LED measured under high and low injection currents, both at room

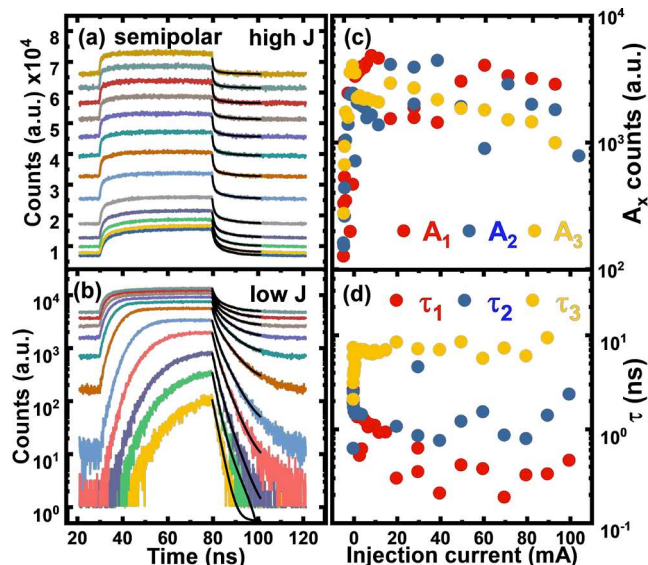


Figure 4. TREL decay traces as a function of injection current for the semipolar LED at high injection (a) and low injection (b). Tri-exponential model fitted to the decay profiles with corresponding amplitudes (c) and extracted time constants (d) as a function of injection current.

temperature, respectively, where the tri-exponential fitting given below is used for each data set.

$$y = A_1 e^{-t/\tau_1} + A_2 e^{-t/\tau_2} + A_3 e^{-t/\tau_3} \quad (2)$$

where τ_1 , τ_2 , and τ_3 refer to the fastest, fast, and slow components along with their corresponding amplitude coefficients A_1 , A_2 , and A_3 , respectively. Each data set is composed of a different DC bias ranging from 50 μ A to 100 mA, and the effect of this DC bias is apparent when observing the baseline counts for each curve. A 500 mV excitation source is added on top of each DC bias using a bias tee so that we can measure recombination dynamics from a steady state as a function of injection current. Between 50 and 200 μ A, the LED does not reach a steady state and exhibits extremely fast fall times after the excitation source from the AWG is switched off. This may be due to the excitation source being comparatively much larger than the DC bias level, resulting in the excitation source negatively biasing the device and briefly creating an artificial current shaping circuit that introduces other dominant recombination mechanisms such as carrier sweep out, exceeding the response time of the system. Therefore, under very low injection current, these mechanisms are out of the scope of this study.

Figure 4c,d shows the extracted lifetimes of the semipolar LED obtained using the tri-exponential model. Above 3 mA, there are three clear lifetimes associated with the EL decay of

the semipolar LED. In general, τ_1 , τ_2 , and τ_3 decrease with the increasing injection current as expected since increasing the current density increases the recombination rate and thus the carrier lifetime. τ_3 , the slowest component, seems to be the most dominant lifetime at lower injection current but then slowly decreases in its contribution with the increasing current, as indicated by Figure 4d. At higher injection, τ_1 becomes the most dominant component, followed closely by τ_2 and then τ_3 . For example, at 50 mA, the extracted lifetimes are 0.40, 1.2, and 8.3 ns for τ_1 , τ_2 , and τ_3 , respectively. The extracted lifetimes for τ_1 and τ_2 are of the same magnitude as those obtained from the TRPL measurements and comparable to other published data on semipolar LEDs.^{11,33} This suggests that this device is not limited by RC effects. The extracted lifetime τ_3 is responsible for carrier transport effects as it is comparable with the LCR meter measurement, that is, the approximation for the RC lifetime.

Figure 5a,b shows results obtained by applying the same tri-exponential model to the c-plane LED under high and low

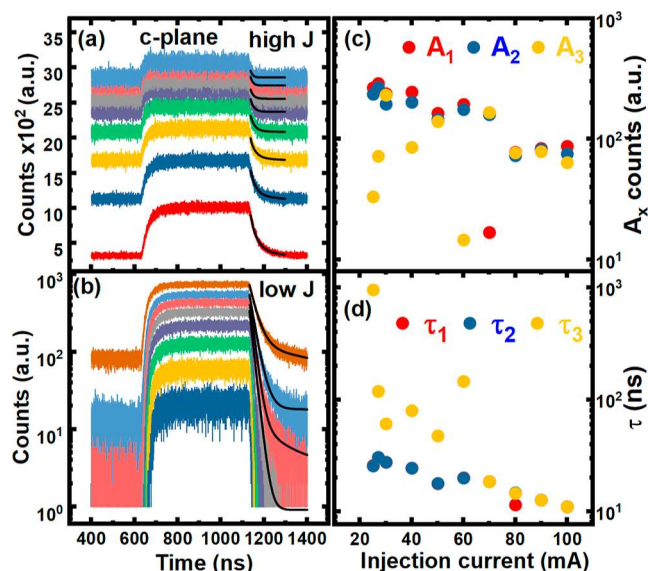


Figure 5. TREL decay traces as a function of injection current for the c-plane LED at high injection (a) and low injection (b). Tri-exponential model fitted to the decay profiles with corresponding amplitudes (c) and extracted time constants (d) as a function of injection current.

injection conditions, respectively. Figure 5c displays the amplitude of each component as a function of injection current, while Figure 5d indicates the lifetime of each component as a function of injection current. τ_1 and τ_2 converge toward a single lifetime of around 12 ns below 60 mA, while τ_3 is a much slower component, exhibiting values between 0.1 and 1 μ s, as shown in Figure 5d. At higher injection, all three lifetimes converge toward a single lifetime that is, a mono-exponential decay, slowly decreasing to 10 ns at 100 mA. LEDs that typically experience a mono-exponential decay are essentially like an RC circuit since the fall time is limited by transport effects. Interestingly, the RC characteristics measured on this device would suggest that the c-plane LED should perform better than the semipolar LED when measuring dynamics. This clearly is not the case, and the reduction in the QCSE present on the semipolar LED has a much more dominant effect on the recombination lifetime and

resulting decay dynamics than the RC measurements, which are expected to be the dominant lifetime with LEDs of this size.

CONCLUSIONS

We have demonstrated the importance of using TREL measurements over TRPL measurements for VLC applications as it is impossible to use TRPL to study transport effects through a LED structure. A detailed comparison study has been conducted by performing TREL and TRPL on a semipolar LED and a c-plane LED both with an emission wavelength in the green spectral region. By performing TREL measurements under bias conditions, the transport effect on carrier lifetime has been studied. The semipolar LED was found to follow closely a tri-exponential decay, with differential carrier lifetimes τ_1 and τ_2 contributing toward radiative and nonradiative recombination, respectively, and τ_3 encapsulating transport effects, while the c-plane LED was reduced to a mono-exponential decay, indicating that τ_{RC} is a limiting factor.

METHODS

LED Fabrication. Two different kinds of green LEDs have been used in the present study: one standard LED on c-plane sapphire and one (11-22) semipolar LED on our high-quality semipolar (11-22) GaN overgrown on m-plane sapphire.^{24,26,34} The c-plane LED consists of seven periods of $\text{In}_{0.25}\text{Ga}_{0.75}\text{N}/\text{GaN}$ MQW structures (well: 2.5 nm and barrier: 13.5 nm). For the semipolar LED, please refer to our previously published papers,^{24,26,34} where a 3 nm single quantum well sandwiched between two 9 nm thick quantum barriers was used as an emitting region for the semipolar LED, and the nominal indium content is 29%. LEDs with a typical dimension of $330 \times 330 \mu\text{m}^2$ have been fabricated using a standard photolithography and dry etching method. A 100 nm thick ITO film was deposited on the top of the device to form a transparent p-contact and then annealed using rapid thermal annealing (RTA). A Ti/Al/Ti/Au stack was thermally evaporated onto the n-GaN to form the n-contact. Finally, Ti/Au was deposited on both contacts to form the p- and n-electrodes.

TREL Measurements. An excitation signal consisting of a 10 MHz (1 MHz for the c-plane LED) square wave with an amplitude of 500 mV (peak-to-peak) is created using an AWG (Tektronix AWG70002A). An identical waveform is created on the adjacent AWG channel and used as a trigger for a TCSPC timing electronics system (Becker & Hickl Simple-Tau 130). The excitation signal is combined with a DC bias from a Keithley 2400 power supply through a 12 GHz bias tee (Tektronix PSPL5575A). A 40 GHz RF probe (FormFactor ACP40-GS300RC) is then used to deliver the resulting RF + DC signal to the LED under test. To monitor the input electrical pulse that includes the effect from the cables, bias tee, and so on, the signal is first connected to a 6 GHz oscilloscope (Tektronix DPO70604C) before the LED. After initial checks, the resulting modulated LED emission is collected through a $50 \times$ magnification, 0.42 NA infinity corrected objective. A 50:50 beam splitter is used to split half the collimated light onto a charge-coupled device (CCD) camera (for aligning, probing, etc.) using a lens tube, while the other half is coupled into a multimode fiber using a parabolic collimator. The light is then dispersed through diffraction grating in a monochromator and then focussed onto a hybrid PMT for TCSPC measurements. A flip mirror is used to switch between the PMT and a

CCD for spectral measurements. Timing synchronization is achieved by combining TCSPC electronics with the falling edge of the trigger signal from the AWG and hybrid PMT measurements.

TRPL Measurements. A pulsed 375 nm laser diode with a 50 ps pulse and a repetition rate of 16 MHz is used as an excitation source. The laser spot size is focused to a 2 μm diameter using an NUV 0.43NA infinity corrected objective lens. The emission is collected through the same lens and coupled into a multimode fiber. The light is then dispersed through a monochromator before focusing onto a hybrid PMT. The overall system has an approximate timing resolution of 15 ps and an instrument response time of 150 ps, which is deconvolved from each measurement.

AUTHOR INFORMATION

Corresponding Author

Tao Wang – Department of Electronic and Electrical Engineering, The University of Sheffield, Sheffield S1 3JD, U.K.; orcid.org/0000-0001-5976-4994; Email: t.wang@sheffield.ac.uk

Authors

Jack Ivan Holly Haggart – Department of Electronic and Electrical Engineering, The University of Sheffield, Sheffield S1 3JD, U.K.; orcid.org/0000-0001-5198-6445

Suneal S. Ghataora – Department of Electronic and Electrical Engineering, The University of Sheffield, Sheffield S1 3JD, U.K.

Valerio Trinito – Department of Electronic and Electrical Engineering, The University of Sheffield, Sheffield S1 3JD, U.K.

Jie Bai – Department of Electronic and Electrical Engineering, The University of Sheffield, Sheffield S1 3JD, U.K.; orcid.org/0000-0002-6953-4698

Complete contact information is available at:

<https://pubs.acs.org/10.1021/acsp Photonics.2c00414>

Author Contributions

T.W. conceived the idea and organized the project. S.G. and J.H. established the TREL system and performed the measurements. J.B. fabricated the devices. V.T. performed TRPL measurements. T.W. and J.H. prepared the manuscript.

Funding

Financial support is acknowledged from the Engineering and Physical Sciences Research Council (EPSRC), UK via EP/P006973/1, EP/T013001/1, and EP/M015181/1

Notes

The authors declare no competing financial interest.

REFERENCES

- (1) Haas, H. LiFi Is a Paradigm-Shifting 5G Technology. *Rev. Phys.* **2018**, *3*, 26–31.
- (2) Minsky, M. S.; Fleischer, S. B.; Abare, A. C.; Bowers, J. E.; Hu, E. L.; Keller, S.; Denbaars, S. P. Characterization of High-Quality InGaN/GaN Multi-Quantum Wells with Time-Resolved Photoluminescence. *Appl. Phys. Lett.* **1998**, *72*, 1066–1068.
- (3) Okur, S.; Nami, M.; Rishinaramangalam, A. K.; Oh, S. H.; DenBaars, S. P.; Liu, S.; Brener, I.; Feezell, D. F. Internal Quantum Efficiency and Carrier Dynamics in Semipolar (20-21) InGaN/GaN Light-Emitting Diodes. *Opt. Express* **2017**, *25*, 2178–2186.
- (4) Okur, S.; Nami, M.; Rishinaramangalam, A. K.; Oh, S. H.; DenBaars, S. P.; Liu, S.; Brener, I.; Feezell, D. F. Internal quantum

efficiency and carrier dynamics in semipolar (20-2-1) InGaN/GaN light-emitting diodes. *Opt. Express* **2017**, *25*, 2178–2186.

(5) Kim, H.; Shin, D.-S.; Ryu, H.-Y.; Shim, J.-I. Analysis of Time-Resolved Photoluminescence of InGaN Quantum Wells Using the Carrier Rate Equation. *Jpn. J. Appl. Phys.* **2010**, *49*, 112402.

(6) Isilm, M. S.; Ferreira, R. X.; He, X.; Xie, E.; Videv, S.; Viola, S.; Watson, S.; Bamiedakis, N.; Penty, R. V.; White, I. H.; Kelly, A. E.; Gu, E.; Haas, H.; Dawson, M. D. Towards 10 Gb/s Orthogonal Frequency Division Multiplexing-Based Visible Light Communication Using a GaN Violet Micro-LED. *Photonics Res.* **2017**, *5*, A35–A43.

(7) Tsonev, D.; Chun, H.; Rajbhandari, S.; Mckendry, J. J. D.; Videv, S.; Gu, E.; Haji, M.; Watson, S.; Kelly, A. E.; Faulkner, G.; Dawson, M. D.; Haas, H.; O'Brien, D. A 3-Gb/s Single-LED OFDM-Based Wireless VLC Link Using a Gallium Nitride μ LED. *IEEE Photonics Technol. Lett.* **2014**, *26*, 637–640.

(8) Xie, E.; Bian, R.; He, X.; Isilm, M. S.; Chen, C.; Mckendry, J. J. D.; Gu, E.; Haas, H.; Dawson, M. D. Over 10 Gbps VLC for Long-Distance Applications Using a GaN-Based Series-Biased Micro-LED Array. *IEEE Photonics Technol. Lett.* **2020**, *32*, 499–502.

(9) Gong, Z.; Jin, S.; Chen, Y.; McKendry, J.; Massoubre, D.; Watson, I. M.; Gu, E.; Dawson, M. D. Size-Dependent Light Output, Spectral Shift, and Self-Heating of 400 Nm InGaN Light-Emitting Diodes. *J. Appl. Phys.* **2010**, *107*, 013103.

(10) Su, Z. C.; Xu, S. J. Effective Lifetimes of Minority Carriers in Time-Resolved Photocurrent and Photoluminescence of a Doped Semiconductor: Modelling of a GaInP Solar Cell. *Sol. Energy Mater. Sol. Cells* **2019**, *193*, 292–297.

(11) Haggart, J. I.; Cai, Y.; Ghataora, S. S.; Smith, R. M.; Bai, J.; Wang, T. High Modulation Bandwidth of Semipolar (11-22) InGaN/GaN LEDs with Long Wavelength Emission. *ACS Appl. Electron. Mater.* **2020**, *2*, 2363–2368.

(12) Rashidi, A.; Nami, M.; Monavarian, M.; Aragon, A.; DaVico, K.; Ayoub, F.; Mishkat-Ul-Masabih, S.; Rishinaramangalam, A.; Feezell, D. Differential Carrier Lifetime and Transport Effects in Electrically Injected III-Nitride Light-Emitting Diodes. *J. Appl. Phys.* **2017**, *122*, 035706.

(13) David, A.; Hurni, C. A.; Young, N. G.; Craven, M. D. Carrier Dynamics and Coulomb-Enhanced Capture in III-Nitride Quantum Heterostructures. *Appl. Phys. Lett.* **2016**, *109*, 033504.

(14) Esquivias, I.; Weisser, S.; Romero, B.; Ralston, J. D.; Rosenzweig, J. Carrier Dynamics and Microwave Characteristics of GaAs-Based Quantum-Well Lasers. *IEEE J. Quantum Electron.* **1999**, *35*, 635–646.

(15) Weisser, S.; Esquivias, I.; Tasker, P. J.; Ralston, J. D.; Romero, B.; Rosenzweig, J. Impedance Characteristics of Quantum-Well Lasers. *IEEE Photonics Technol. Lett.* **1994**, *6*, 1421–1423.

(16) Rashidi, A.; Monavarian, M.; Aragon, A.; Feezell, D. Exclusion of Injection Efficiency as the Primary Cause of Efficiency Droop in Semipolar (20-2-1) InGaN/GaN Light-Emitting Diodes. *Appl. Phys. Lett.* **2018**, *113*, 031101.

(17) Viola, S.; Isilm, M. S.; Watson, S.; Videv, S.; Haas, H.; Kelly, A. E. 15 Gb/s OFDM-Based VLC Using Direct Modulation of 450 GaN Laser Diode. *Proceedings 10437, Advanced Free-Space Optical Communication Techniques and Applications III*, 2017; p 104370E.

(18) Lee, C.; Zhang, C.; Cantore, M.; Farrell, R.; Oh, S. H.; Margalith, T.; Speck, J. S.; Nakamura, S.; Bowers, J. E.; DenBaars, S. P. 2.6 GHz High-Speed Visible Light Communication of 450 Nm GaN Laser Diode by Direct Modulation. *IEEE Summer Topical Meeting Series*, 2015; pp 112–113.

(19) Chi, Y.-C.; Hsieh, D.-H.; Tsai, C.-T.; Chen, H.-Y.; Kuo, H.-C.; Lin, G.-R. 450-Nm GaN Laser Diode Enables High-Speed Visible Light Communication with 9-Gbps QAM-OFDM. *Opt. Express* **2015**, *23*, 13051–13059.

(20) Bernardini, F.; Fiorentini, V.; Vanderbilt, D. Spontaneous Polarization and Piezoelectric Constants of III-V Nitrides. *Phys. Rev. B: Condens. Matter Mater. Phys.* **1997**, *56*, R10024.

(21) Takeuchi, T.; Amano, H.; Akasaki, I. Theoretical Study of Orientation Dependence of Piezoelectric Effects in Wurtzite Strained

GaN/InGaN Heterostructures and Quantum Wells. *Jpn. J. Appl. Phys.* **2000**, *39*, 413–416.

(22) Wang, S.-W.; Chen, F.; Liang, L.; He, S.; Wang, Y.; Chen, X.; Lu, W. A High-Performance Blue Filter for a White-Led-Based Visible Light Communication System. *IEEE Wireless Commun.* **2015**, *22*, 61–67.

(23) Northrup, J. E. GaN and InGaN (11-22) Surfaces: Group-III Adlayers and Indium Incorporation. *Appl. Phys. Lett.* **2009**, *95*, 133107.

(24) Wang, T. Topical Review: Development of Overgrown Semi-Polar GaN for High Efficiency Green/Yellow Emission. *Semicond. Sci. Technol.* **2016**, *31*, 093003.

(25) Hagggar, J. I. H.; Cai, Y.; Bai, J.; Ghataora, S.; Wang, T. Long-Wavelength Semipolar (11–22) InGaN/GaN LEDs with Multi-Gb/s Data Transmission Rates for VLC. *ACS Appl. Electron. Mater.* **2021**, *3*, 4236–4242.

(26) Bai, J.; Xu, B.; Guzman, F. G.; Xing, K.; Gong, Y.; Hou, Y.; Wang, T. (11-22) semipolar InGaN emitters from green to amber on overgrown GaN on micro-rod templates. *Appl. Phys. Lett.* **2015**, *107*, 261103.

(27) Schubert, E. F. *Light-Emitting Diodes*, 3rd ed.; Cambridge University Press, 2018.

(28) Kawakami, Y.; Suzuki, S.; Kaneta, A.; Funato, M.; Kikuchi, A.; Kishino, K. Origin of High Oscillator Strength in Green-Emitting InGaN/GaN Nanocolumns. *Appl. Phys. Lett.* **2006**, *89*, 163124.

(29) Liu, B.; Smith, R.; Athanasiou, M.; Yu, X.; Bai, J.; Wang, T. Temporally and Spatially Resolved Photoluminescence Investigation of (1122) Semi-Polar InGaN/GaN Multiple Quantum Wells Grown on Nanorod Templates. *Appl. Phys. Lett.* **2014**, *105*, 261103.

(30) Chen, S.-W. H.; Huang, Y.-M.; Chang, Y.-H.; Lin, Y.; Liou, F.-J.; Hsu, Y.-C.; Song, J.; Choi, J.; Chow, C.-W.; Lin, C.-C.; Horng, R.-H.; Chen, Z.; Han, J.; Wu, T.; Kuo, H.-C. High-Bandwidth Green Semipolar (20–21) InGaN/GaN Micro Light-Emitting Diodes for Visible Light Communication. *ACS Photonics* **2020**, *7*, 2228–2235.

(31) Bhattacharya, P.; Frost, T.; Deshpande, S.; Baten, M. Z.; Hazari, A.; Das, A. Room Temperature Electrically Injected Polariton Laser. *Phys. Rev. Lett.* **2014**, *112*, 236802.

(32) Feng, S.-W.; Cheng, Y.-C.; Liao, C.-C.; Chung, Y.-Y.; Liu, C.-W.; Yang, C.-C.; Lin, Y.-S.; Ma, K.-J.; Chyi, J.-I. Two-Component Photoluminescence Decay in InGaN/GaN Multiple Quantum Well Structures. *Phys. Status Solidi A* **2001**, *228*, 121–124.

(33) Monavarian, M.; Rashidi, A.; Aragon, A. A.; Oh, S. H.; Rishinaramangalam, A. K.; DenBaars, S. P.; Feezell, D. Impact of Crystal Orientation on the Modulation Bandwidth of InGaN/GaN Light-Emitting Diodes. *Appl. Phys. Lett.* **2018**, *112*, 041104.

(34) Zhang, Y.; Smith, R. M.; Hou, Y.; Xu, B.; Gong, Y.; Bai, J.; Wang, T. Stokes Shift in Semi-polar (11-22) InGaN/GaN Multiple Quantum Wells. *Appl. Phys. Lett.* **2016**, *108*, 031108.

Recommended by ACS

Finite-Size Effects on Energy Transfer between Dopants in Nanocrystals

Mark J. J. Mangnus, Freddy T. Rabouw, *et al.*

NOVEMBER 08, 2021
ACS NANOSCIENCE AU

READ 

Excited State Absorption for Ratiometric Thermal Imaging

Joanna Drabik and Lukasz Marciniak

DECEMBER 22, 2020
ACS APPLIED MATERIALS & INTERFACES

READ 

Impact of Noise and Background on Measurement Uncertainties in Luminescence Thermometry

Thomas P. van Swieten, Freddy T. Rabouw, *et al.*

MARCH 11, 2022
ACS PHOTONICS

READ 

Multiplasmons-Pumped Excited-State Absorption and Energy Transfer Upconversion of Rare-Earth-Doped Luminescence beyond the Diffraction Limit

Huan Chen, Hongxing Xu, *et al.*

MARCH 04, 2021
ACS PHOTONICS

READ 

Get More Suggestions >